An Investigation of the Initial Development of the Double-ITCZ Warm SST Biases in the CCSM

HAILONG LIU

State Key Laboratory of Atmospheric Sciences and Geophysical Fluid Dynamics, Institute of Atmospheric Physics, Chinese Academy of Sciences, Beijing, China

MINGHUA ZHANG AND WUYIN LIN

Institute for Terrestrial and Planetary Atmospheres, Stony Brook University, Stony Brook, New York

(Manuscript received 13 August 2010, in final form 7 April 2011)

ABSTRACT

This paper investigates the initial development of the double ITCZ in the Community Climate System Model version 3 (CCSM3) in the central Pacific. Starting from a resting initial condition of the ocean in January, the model developed a warm bias of sea surface temperature (SST) in the central Pacific from 5°S to 10°S in the first three months. This initial bias is caused by excessive surface shortwave radiation that is also present in the stand-alone atmospheric model. The initial bias is further amplified by biases in both surface latent heat flux and horizontal heat transport in the upper ocean. These biases are caused by the responses of surface winds to SST bias and the thermocline structure to surface wind curls. This study also showed that the warming biases in surface solar radiation and latent heat fluxes are seasonally offset by cooling biases from reduced solar radiation after the austral summer due to cloud responses and in the austral fall due to enhanced evaporation when the maximum SST is closest to the equator. The warming biases from the dynamic heat transport by ocean currents however stay throughout all seasons once they are developed, which are eventually balanced by enhanced energy exchange and penetration of solar radiation below the mixed layer. It was also shown that the equatorial cold tongue develops after the warm biases in the south-central Pacific, and the overestimation of surface shortwave radiation recurs in the austral summer in each year. The results provide a case study on the physical processes leading to the development of the double ITCZ. Applicability of the results in other models is discussed.

1. Introduction

The central Pacific double intertropical convergence zone (ITCZ) in coupled ocean–atmosphere models refers to two rainfall belts symmetric with respect to the equator from around 160°E to 160°W. In observations, the double ITCZ only appears in the boreal spring; in other seasons only one band of maximum rainfall exists to the north of the equator. In coupled ocean–atmosphere models, however, the southern maximum appears throughout the year (Mechoso et al. 1995). Associated with this spurious double ITCZ are the symmetric distributions across the equator of sea surface temperature (SST), zonal currents, upwelling, and thermocline (e.g., Zhang et al. 2007). After it was identified as a systematic bias in climate models, many studies have tried to eliminate it since it has serious consequences on the ability of a model to realistically simulate tropical mean climate, El Niño events, and teleconnection patterns. The problem, however, is still evasive, as it has been shown to exist in almost all climate models participating in the most recent Intergovernmental Panel on Climate Change (IPCC) Fourth Assessment Report (AR4) models (Lin 2007).

In the literature, a double-ITCZ-related warm SST bias is often broadly referred to as the spurious warm water band south of the equator from the central Pacific to the west coast of South America. From the process perspective however, there are two distinct regions with different controlling processes: in the central Pacific where a deep convection and precipitation appears south of the equator in models and in the eastern Pacific where a maximum bias of SST occurs. The latter is believed to be related to a deficient amount of low stratus and stratocumulus clouds (Ma et al. 1996; Yu and Mechoso 1999; Dai et al. 2003).

Corresponding author address: Hailong Liu, No. 40, Hua Yan Li, Beijing 100029, China.
E-mail: lhl@lasg.iap.ac.cn

DOI: 10.1175/2011JCLI4001.1

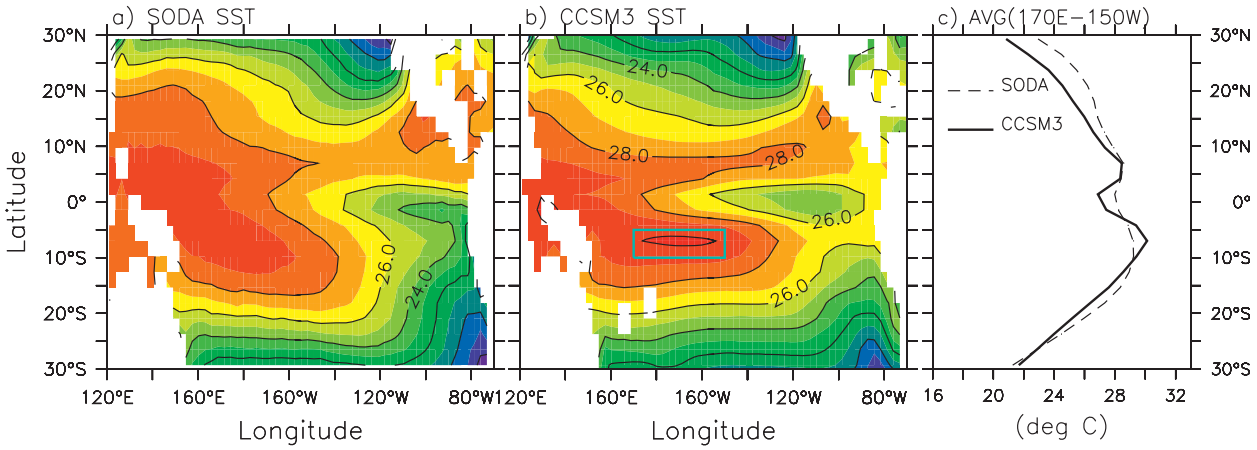

FIG. 1. Annual mean sea surface temperature (°C) for (a) SODA (1993–2004) and (b) CCSM ensemble mean (years 6–10) and (c) the zonal averaged SSTs between 170°E and 150°W for SODA (dash) and CCSM (solid). The box in (b) from 5° to 10°S, 170° to 150°E denotes the domain in which the heat budget is computed.

In the central Pacific, the spurious maximum of convection locks the surface winds, SST, and ocean currents into a biased pattern through a wind–convection feedback (e.g., Zhang 1996; Zhang et al. 2007; Song and Zhang 2009). In this study, we focus on the region of the double ITCZ in the central Pacific from 5°S to 10°S, 170°E to 150°W denoted by the rectangular box in Fig. 1. Although this is not the region in which SST suffers the largest error in coupled models (Xie and Philander 1994), it is where the anomalous deep convection occurs that can have large impact on climate in remote regions.

Zhang et al. (2007) proposed a positive feedback loop to explain the possible mechanism of triggering and eastward propagation of the positive precipitation errors in this region. They hypothesized that the loop starts from a positive perturbation of precipitation around the date line between 5° and 10°S. Then the latent heating leads to a strong convergence of the surface winds toward the precipitation region. The changed wind pattern leads to an upwelling due to the Ekman pumping immediately south of the initial precipitation region. The anomalous upwelling raises the thermocline ridge, resulting in a meridional thermocline slope across the target region that drives a spurious eastward Southern Equatorial Counter Current (SECC) just coinciding with the precipitation anomaly. Consequently, the precipitation anomaly propagates eastward following the positive SST anomaly, which is advected by the anomalous eastward ocean current. This process closes the whole loop. In this hypothesis, the role of ocean dynamics in the development of the double ITCZ has been explicitly brought up for the first time in the literature. Recently, Zhang and Song (2010) also suggested that ocean heat transport is largely responsible for the warm SST bias in the central equatorial Pacific, especially during boreal summer. The results used in both studies however were from the equilibrium state of the model integration. The initial and the ensuing developing processes, which is in the hypothesis of Zhang et al. (2007), have not been demonstrated in the analysis of the equilibrium states.

The purpose of the present study is to describe and interpret the physical processes responsible for the initial development of the double-ITCZ-related warm SST bias in the Community Climate System Model version 3 (CCSM3). We will demonstrate the initial processes and the role of ocean dynamics in the development of a double ITCZ in the central Pacific. Given that the double-ITCZ bias has been a long-standing problem in coupled models, our goal is to present a case study to aid in the eventual elimination of this bias.

This paper is organized as follows. Section 2 describes the model, the experiments, the heat budget analysis method, and the datasets that we used. Section 3 presents some key features of the development of SST biases in the CCSM, an analysis of the physical processes, and results from a sensitive experiment. The last section contains a summary and discussion.

2. Model, method, and datasets

a. Model and experiments

The model employed in this study is the standard CCSM3 (Collins et al. 2006a). The component models include the Community Atmosphere Model version 3.1 (CAM3.1) (Collins et al. 2004, 2006b), the Community Land Surface Model version 3 (CLM3) (Oleson et al. 2004; Dickinson et al. 2006), the Community Sea Ice Model version 5 (CSIM5) (Briegleb et al. 2004), and the Parallel Ocean Program version 1.4.3 (POP) (Smith and

Gent 2002). An intermediate resolution configuration is chosen, which combines the T42 CAM/CLM with the 1° POP/CSIM. The vertical dimensions are 26 levels for the atmosphere and 40 levels for ocean. More details about CCSM3 can be found in Collins et al. (2006a). CCSM3 included new model physics to reduce some biases, but the double-ITCZ bias still exists (Collins et al. 2006a); this is also the case in the newly released CCSM4 with both the fourth and fifth versions of the CAM (e.g., Gent et al. 2011).

In the present study, we focus on the first one to two years of the integration. Therefore, the magnitude and/or timing of the model systematic errors might be influenced by initial condition and the internal variability of the coupled model itself. To minimize this effect, an ensemble of five 10-yr integrations is conducted under the present-day condition using CCSM3. The CAM/CLM started from initial conditions obtained from the Atmospheric Model Intercomparison Project (AMIP) integration, while the POP/CSIM started from Levitus temperature (Levitus and Boyer 1994) and salinity (Levitus et al. 1994) merged with the Poles Arctic-Ocean dataset (http://psc.apl.washington.edu/Climatology.html) in January. The oceanic currents are set to be zero, as well as the velocities of sea ice. We can, therefore, investigate the development of the SST biases by comparing the model simulations with observations. The monthly ensemble mean is used to analyze the simulation results. To identify processes related to the atmospheric general circulation model (AGCM), the CAM AMIP integrations from the CCSM Atmospheric Model Working Group (http://www.ccsm.ucar.edu/models/atm-cam/sims/cam3.0/) are also used to compare with simulations from the coupled model.

A sensitivity experiment is also conducted to investigate the impact of surface radiation by perturbing a parameter in the convection scheme (Zhang and McFarlane, 1995) that describes the conversion of cloud water to rainwater as follows:

$$\rho R_u = c_0 M_u l, \tag{1}$$

where ρ stands for air density; R_u is the conversion from the cloud liquid water to rainwater in the updraft; M_u is the ensemble cloud updraft mass flux; and l is the cloud liquid water content; c_0 is the conversion parameter, taken to be 3×10^{-3} m^{-1} by default. In the perturbed experiment, which is named "c0 experiment" hereafter, c0 is reduced to 1×10^{-3} m^{-1} in the tropics (30°S–30°N). Based on (1), the smaller value of c_0 slows the conversion of cloud water to rainwater, thereby resulting in more liquid water in clouds and less downward shortwave radiation at the surface.

b. Datasets

In a previous study (Liu et al. 2010), we compared seven objective analyses of surface fluxes and four ocean data assimilation products over the central equatorial Pacific and evaluated them against field observations. We have concluded that the Simple Ocean Data Assimilation version 2 (SODA2; Carton and Giese 2008), the new Global Ocean Data Assimilation System (GODAS; Behringer and Xue 2004), and the Estimating the Circulation and Climate of the Ocean-Global Ocean Data Assimilation Experiment (ECCO-GODAE) at the Massachusetts Institute of Technology, version 2 (http://www.ecco-group.org/) (Wunsch and Heimbach 2007) are all suitable to describe the surface net flux and horizontal heat transport over the region of the double ITCZ. Since SODA has both a longer duration (1958–2007) and higher horizontal resolution (0.5° by 0.5°) than the other two products, the monthly mean temperature, three-dimensional velocity, and net surface heat flux from SODA between 1993 and 2004 are used to compute the climatology of the heat budget over the south-central equatorial Pacific in the present study. Calculation using GODAS in the same period shows no qualitative differences from SODA. To confirm consistency among the observational datasets, SST and the surface wind stresses from SODA are used to evaluate the model output as well. Also based on Liu et al. (2010), the surface shortwave and latent heat flux from the adjusted National Ocean Center Southampton (NOCS) fluxes climatology (Grist and Josey 2003) are used to validate the individual surface heat flux components in CCSM3.

In addition, the climatology of the total cloud amount from International Satellite Cloud Climatology Project (ISCCP D2; Rossow et al. 1996) and the total cloud liquid water path from Special Sensor Microwave Imager (SSM/I; Wentz 1997) are used to evaluate the model results. The former is averaged from July 1983 to September 2001, and the latter from January 1987 to December 2000.

c. Mixed layer heat budget calculation

To compare with the monthly mean oceanic analysis data, the heat budget of the model is also calculated offline using the monthly model output. The equation governing ocean mixed layer temperature, when it is spatially integrated over the study domain and temporally integrated in a month, can be written as

$$\iint\left(\rho_0 C_p h \frac{\partial\langle\overline{T}\rangle}{\partial t}\right)dx\,dy = \iint\left(-\rho_0 C_p h\left\langle\frac{\partial\overline{u}\,\overline{T}}{\partial x}+\frac{\partial\overline{v}\,\overline{T}}{\partial y}\right\rangle+\overline{Q_0}-\overline{Q_{\text{pen}}}+R\right)dx\,dy. \tag{2}$$

For simplicity, only five terms are kept in the equation, namely, the time tendency of the mixed layer temperature,

horizontal advection over the mixed layer, the net surface heat flux, the solar radiation penetrating the bottom of the mixed layer, and the residual R. In (2) the angle brackets and bars denote the vertical average over the mixed layer and the temporal average in a month; T, u, and v are temperature, zonal current, meridional current, and vertical current, respectively; h is the mixed layer depth; Q_0 and Q_{pen} are the net surface heat flux and the solar radiation penetrating the bottom of the mixed layer; Q_0 is the sum of surface latent and sensible heat fluxes as well as longwave and shortwave radiative fluxes; ρ_0 (1026 km m^{-3}) and C_p [3996 J (kg K)$^{-1}$] are the reference oceanic density and the specific heat of seawater, respectively; and R represents the residual term, which includes entrainment, the subgrid nonlinear terms from the horizontal advection term. Calculation with daily mean model output shows little difference from the results with monthly mean output, so monthly data are used in the following analysis.

In calculating the horizontal advection term, the method of Lee et al. (2004) is used; their formulation is expressed as advection of interface temperature referenced to the spatially averaged temperature of the study domain. The volume-averaged temperature of the target domain is used as the reference temperature.

The flux Q_{pen} is estimated by using the empirical formula of Paulson and Simpson (1977):

$$Q_{\text{pen}}(z) = Q_{\text{sw}} \times [Re^{-z/z_1} + (1 - R)e^{-z/z_2}] \quad (3)$$

The two terms on the right-hand side of (3) represent the percentage of solar radiation penetrated below a certain depth, z, in the infrared band and the ultraviolet and visible band, respectively. Following the Rosati and Miyakoda (1988), we used the values $R = 0.58$, $z_1 = 0.35$ m, and $z_2 = 23$ m. In CCSM, a chlorophyll-dependent scheme is chosen. But because the concentration of chlorophyll in this region is around 0.1 mg m^{-3}, the transmission functions of the two methods are almost identical (e.g., Lin et al. 2007, their Fig. 2).

The mixed layer is defined in the present study as the depth at which the temperature is 0.5°C lower than SST. Alternative definitions can be used, such as a fixed depth. These will primarily affect the penetration of solar radiation and subgrid-scale mixing at the bottom of the mixed layer, but not surface fluxes and horizontal heat transport by ocean currents that will be presented.

3. Results

a. Development of SST biases in the south-central equatorial Pacific

The SST biases in the tropical Pacific Ocean developed within two years in the CCSM3, and after five years the biases become almost the same as has been reported in previous studies in climatological simulations (e.g., Collins et al. 2006a; Large and Danabasoglu 2006; Zhang et al. 2007; Lin 2007). Figures 1a and 1b compare the SST in observation and simulation averaged from years 6 to 10. The most prominent features of the biases in the central Pacific, common also to other coupled models, are the two narrow maximum SST bands symmetric with respect to the equator and the extended cold tongue along the equator. The spurious warm water south to the equator between 10° and 5°S, about 1°–2°C warmer than the observation and highlighted by the rectangular box, between 5° and 10°S, in Fig. 1b, will be the primary focus of this study.

Besides the warm bias, CCSM also produced cold biases south of 10°S. These biases can be more clearly seen in the zonally averaged SST from 170°E to 150°W (Fig. 1c). The cold biases at southern latitudes narrow the warm pool and change its orientation from northwest–southeast to west–east. The meridional temperature gradient to the south of the study domain is also intensified. The cold biases at the equator are associated with the westward extension of the cold tongue in the simulation. These two cold biases at the equator and south of 10°S are both common problems in coupled models (e.g., Lin 2007).

Figure 2 shows the development of the double ITCZ in the first five years of the integration (thick solid) along with the quasi-equilibrium state of the model result (thin solid) and observation (dashed). The warm bias in the south-central equatorial Pacific occurs in the very first year, in which the magnitude of warm bias is as large as in the equilibrium state. The location of the warmest water is slightly to the north in the first year relative to that in subsequent years. Figure 2 also shows the year-to-year variation of the cold biases south of 10°S and at the equator. The former is fully developed in the first year, while the later reaches equilibrium after 2–3 years of adjustment.

To better understand the biases in the annual means, we show the seasonal variation of the zonally averaged SST over 170°E–150°W in Fig. 3 from the simulation (contour) and the observation (shaded), for the first two years in Fig. 3a, and for the average of years 6–10 in Fig. 3b. There is a clear seasonal cycle of SST south of the equator, with maximum temperature in the austral summer and fall (boreal winter and spring), following the seasonal march of the sun with about two-month delay.

SST in the model is initially similar to the observation, but a warm bias of 1°–2° develops in the first three months from the equator to 10°S. In observation, SST changes from 29.5°C in southern summer to about 28.5°C in southern winter. But in the model, SST changes from

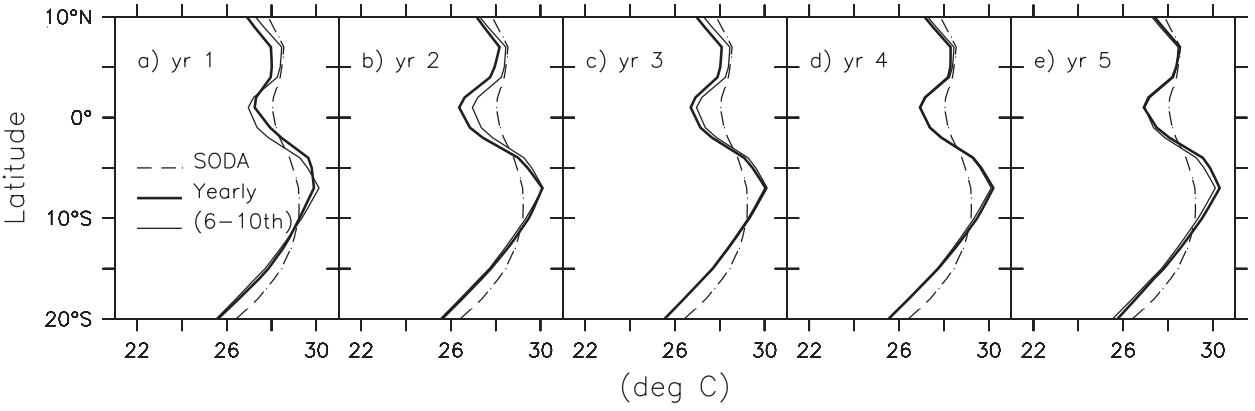

FIG. 2. Sea surface temperatures (°C) averaged between 170°E and 150°W for the first five individual years of the CCSM ensemble mean (thick), the average of years 6–10 of CCSM (thin), and the climatology of SODA during 1993–2004 (dash).

over 30°C to around 29.5°C. A band of warm SST above 29.5°C, centered on 5°S, remains through the austral winter. The warm SST of this band is increased again in the following September to February as the warm water expands southward.

The cold bias south of 10°S that has developed by May in the first year persists throughout the rest of the year. This cold bias and the warm bias to the north set up a large meridional gradient of SST over the south-central equatorial Pacific in the simulation that affects the surface winds and the latent heat flux.

The SST seasonal cycle in the second year is similar to the first year, except for the earlier emergence of the 30°C isotherm as a result of excess solar radiation in the first calendar year south of the equator. An even warmer center above 30.5°C occurs in February. This indicates that the warm biases are still developing in the austral summer of the second year.

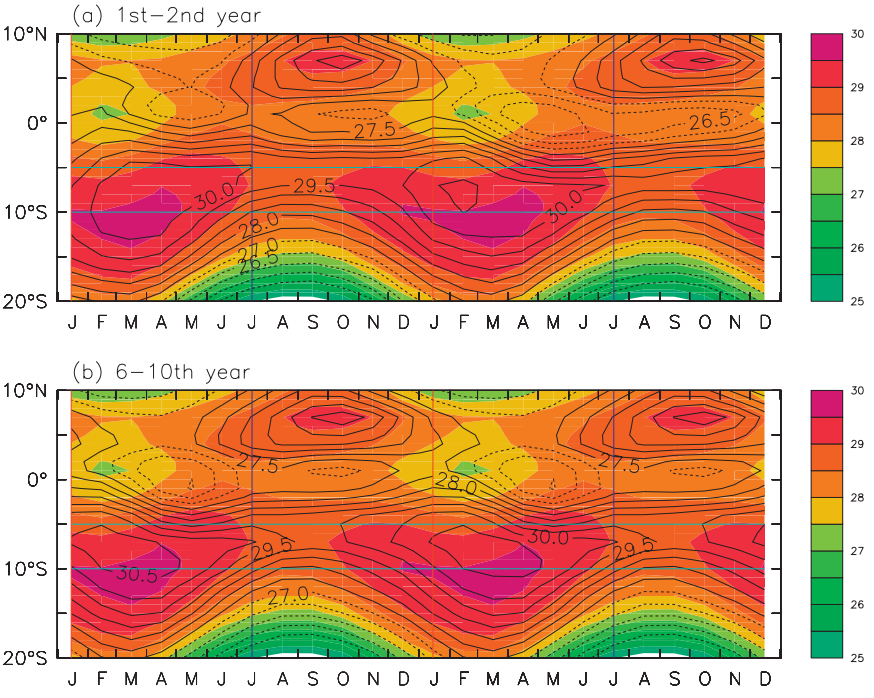

FIG. 3. Time–latitude diagrams of zonal mean temperature between 170°E and 150°W for (a) the first two years and (b) the climatology of years 6–10 of CCSM ensemble mean (contour, in °C). The shaded is from the climatology of SODA during 1993–2004. The beginning of January and July of each year is marked in red and blue, respectively. The region between the two horizontal lines at 5° and 10°S denotes the study domain.

Another distinct feature in the second year is the setup of the cold tongue at the equator. The SST at the equator is below 27°C almost all year long. This cold tongue confines the warm water above 30°C to the south of 5°S in subsequent seasons. The development of the cold tongue suggests a dynamic response of the equatorial ocean associated with excessive upwelling.

The seasonal variation of the warm SST in subsequent years is almost identical to that in the second year (Fig. 3b). The cold biases south of 10°S are also similar to those in the first and second years. The cold tongue along the equator remains throughout the season, with a semiannual cycle of minimum SST in the two equinox transition seasons. This is in contrast to the annual cycle of equatorial SST in observation that has a minimum (maximum) in the boreal winter (summer). This problem is common to CCSM3 and its previous versions (Large and Danabasoglu 2006).

As shown above, the warm biases in the south-central equatorial Pacific develop rapidly in the first two years of integration. What processes cause and maintain the narrow warm band in the Southern Hemisphere? This will be explored next.

b. Time evolution of the heat budget

To evaluate model results against observational data, we use the estimate of the annual mean mixed layer heat budget in the south-central equatorial Pacific from Liu et al. 2010, which is shown in Table 1. In observation, the 7 W m^{-2} surface heating is primarily balanced by the horizontal zonal advection of 5 W m^{-2}, which is due to cold water transported by the westward South Equatorial Current (SEC) and a smaller loss of solar radiation penetration of 3 W m^{-2}. In the model, there is a warming of 0.6°C in the first year. Associated with the warming is the large surface heat flux and horizontal transport by ocean currents. In subsequent years, the model surface heat flux bias is diminished, but the bias in advective tendency remains, which is balanced by more shortwave penetration due to a shallower mixed layer, subgrid-scale mixing and vertical temperature transport. In the advective transport of heat, both zonal and meridional components contribute to the warming.

The development of the warm bias is most clearly seen in Fig. 4, which compares the rate of change of the mixed layer ocean temperature in the model (solid) against observation (dashed) for the study domain in the first two years and in the average of the last five years. We are focusing on the difference between the solid and dashed lines, which measures the cooling or warming biases in the model. The model largely overestimates the warming in the first two months in the first year, about 60 W m^{-2} in January and 30 W m^{-2} in February. After that, the warming decreases rapidly and becomes a cooling bias in March. Starting from the second year, there is also a large warming bias in the model in austral summer. This is followed by cooling in the equinox seasons, with relatively minimum differences in the austral winter (June–August).

TABLE 1. Annual-mean mixed layer heat budget over the south-central equatorial Pacific from obsevations (Obs), Liu et al. (2010), and for the CCSM ensemble mean in the first, second, and equilibrium years (W m^{-2}). The vertical averaged temperature (°C) and mixed layer depths (MLD; m) are also shown. The residual term is different from Liu et al. since the shortwave radiation penetration has been explicitly computed in present study.

		CCSM		
	Obs	(First year)	(Second year)	(6th–10th year)
$\langle T \rangle$ (°C)	29.0	29.6	29.7	29.7
MLD (m)	81.7	54.5	52.6	50.9
Temp. tendency	0	6	−3	−3
Surface flux	7	10	5	8
SW penetration	−3	−9	−10	−10
Hor. advection (X/Y)	−4.8 (−5/0.2)	8 (−3/11)	6 (−1/7)	8 (−1/9)
Residual	0.8[1]	−3	−4	−9

To understand the cause of this difference, we use Fig. 4 to compare the differences of net downward surface shortwave radiation (Fig. 5a) and surface latent heat flux (Fig. 5b), the two leading terms of surface energy fluxes. Both surface shortwave radiation and latent heat fluxes contribute to the initial warming in the first two months of the simulation, but the shortwave is dominant. After the first year, the seasonal bias in the shortwave radiation is similar to that in the total surface heat flux, particularly the warming bias in austral summer and the subsequent cooling in austral fall. The warming due to latent heat flux is established rapidly in the first month. The warming bias of the latent heat flux maximizes in austral summer, augmenting the warming bias due to solar radiation. This seasonality is because of the reduction of surface wind speed that converges toward the warm water.

It is consistent with the present study that Zhang and Wang (2006) also attributed the initial development of large warm SST biases in the central-south equatorial Pacific to the excessive surface solar radiation. Comparing the differences of the net surface heat flux between their work (their Fig. 3c) and ours (not shown, but almost the same as the solar radiation, Fig. 5a), we found that, although there are differences in other seasons, the magnitude of the positive anomalies in austral summer are about the same. The inconsistency in other seasons is mainly due to the reference that they used is another experiment, not the observation as in this study.

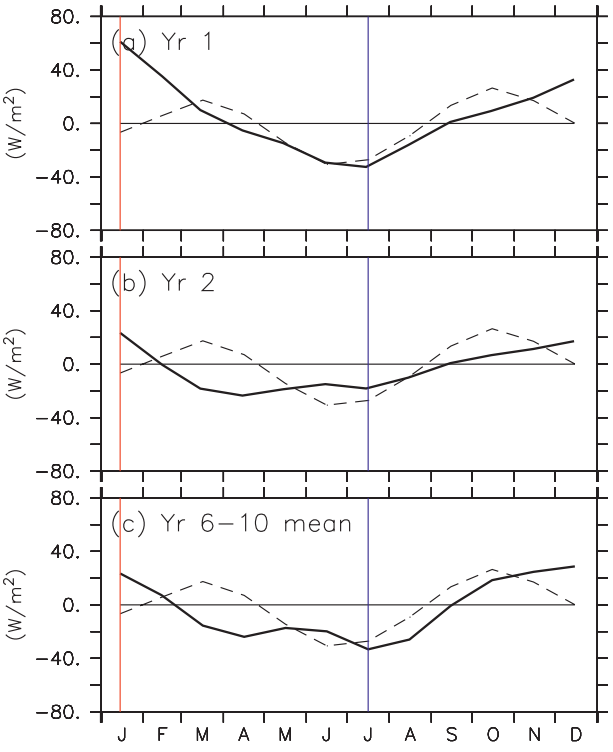

FIG. 4. Monthly mean rate of change of the mixed layer temperature over the study domain for (a) year 1, (b) year 2, and (c) years 6–10 mean of the CCSM ensemble mean (thick, W m^{-2}). The dashed lines are from the climatology of SODA during 1993–2004. January (July) of each year is marked in red (blue).

The excessive shortwave radiation in January and February is followed by underestimation of shortwave radiation due to cloud responses, and the small latent heat flux in this season is partially offset by the excessive cooling of the latent heat flux after the austral winter when the maximum SST moves northward toward the equator. Hence, the annually averaged net heat flux due to the shortwave radiation and latent heat flux are close to observation after the first year, and cannot account for the simulated warming (Table 1).

An additional role is played by the dynamic transport of ocean heat. This is shown in Fig. 6a for the advective tendency in the zonal direction and Fig. 6b in the meridional direction. The warming bias, relative to the cooling in observation, develops in the model in the first month due to the zonal transport; this bias then persists throughout the first year and subsequent years (Fig. 6a). A close examination shows that the warming bias in the first half of the year is largely due to the reduced zonal gradient in SST, while the subsequent warming bias is due to the spurious eastward current in the study domain.

Figure 7a shows the time evolution of the zonal current averaged between 10° and 5°S in observation (shade) and in the model (contour). In observation, the zonal current is westward most of the time except in the northern winter to the west of the date line, and this current advects cold water westward. In CCSM however, an eastward current develops after the austral winter of the first year that prevails throughout the year west of 150°W. This current tends to move warm water eastward.

The cause of the eastward current is due to a bias of the thermocline that is initiated by the SST bias. This is shown in Fig. 8. Figures 8a and 8b compare the surface wind and wind curls from SODA with that from the model in the first July of the integration. The spurious convergent surface winds toward the warm SST around the study domain in the model are also associated with negative wind curls. The biases in wind curl cause upwelling and ridging of the thermocline south of the study domain in the model as shown in Fig. 8d, which is compared with observation in Fig. 8c. A spurious eastward current is therefore expected as a result of the geostrophic balance (Fig. 8d). This eastward current is fully developed in the second year of model integration (Fig. 7a).

These results are consistent with the hypothesis in Zhang et al. (2007) from the equilibrium simulations. It takes about eight months for the spurious eastward currents to establish in response to the surface wind stress, which will be shown later. Beside the currents, the changes of the zonal temperature gradient contribute to the initial zonal advective warming biases in CCSM. During the austral summer and fall in the first year, the excessive shortwave radiation warms the water south of the equator from 160°E to 160°W and substantially homogenizes temperature in the zonal direction (Fig. 7b). This reduces the westward transport of cold water.

In addition to the warming bias in the zonal heat transport, a large positive meridional advection develops after boreal summer with a maximum of about 40 W m^{-2} in the simulation (Fig. 6b). As shown in Fig. 3, in boreal summer, the maximum SST is at the northern edge of the study domain around 5°S, therefore the southward meridional current causes positive temperature advection. This is shown in Fig. 9 for the meridional current averaged between 170°E and 150°W in the mixed layer and the ocean temperature in July in the first year of the simulation. In observation, there is very little temperature gradient, as shown by the dashed lines in the figure.

Figure 9a shows a large meridional divergence within the 5°–10°S band, which cannot be found in the SODA data. But the zonal convergence between 170°E and 150°W in July can only partially balance the meridional divergence (Fig. 7a). That indicates an entrainment occurs at the bottom of the mixed layer in the study domain. The entrainment, which dominates the residual term, brings the cold water from below and shoals the mixed layer. The anomalous meridional divergence and

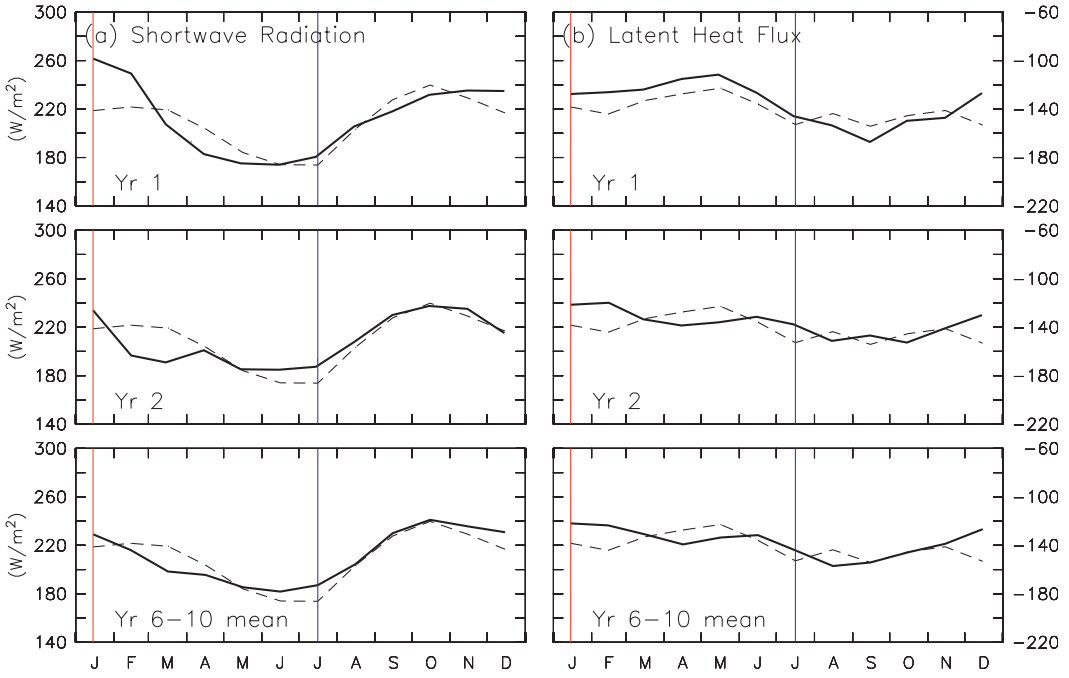

FIG. 5. As in Fig. 4 but for (a) shortwave radiation and (b) latent heat flux. The observation is from NOCS1a.

compensating entrainment are both associated with the anomalous negative surface wind curl in response to excessive meridional gradient of SST in the study domain (not shown).

Unlike the annually averaged biases in surface fluxes, which offset each other in different seasons, the warming biases of the dynamic transport of heat by the ocean currents exist throughout the years to maintain the double ITCZ. They are compensated by greater penetration of shortwave radiation because of the shallower mixed layer and greater mixing with cold water below (Table 1).

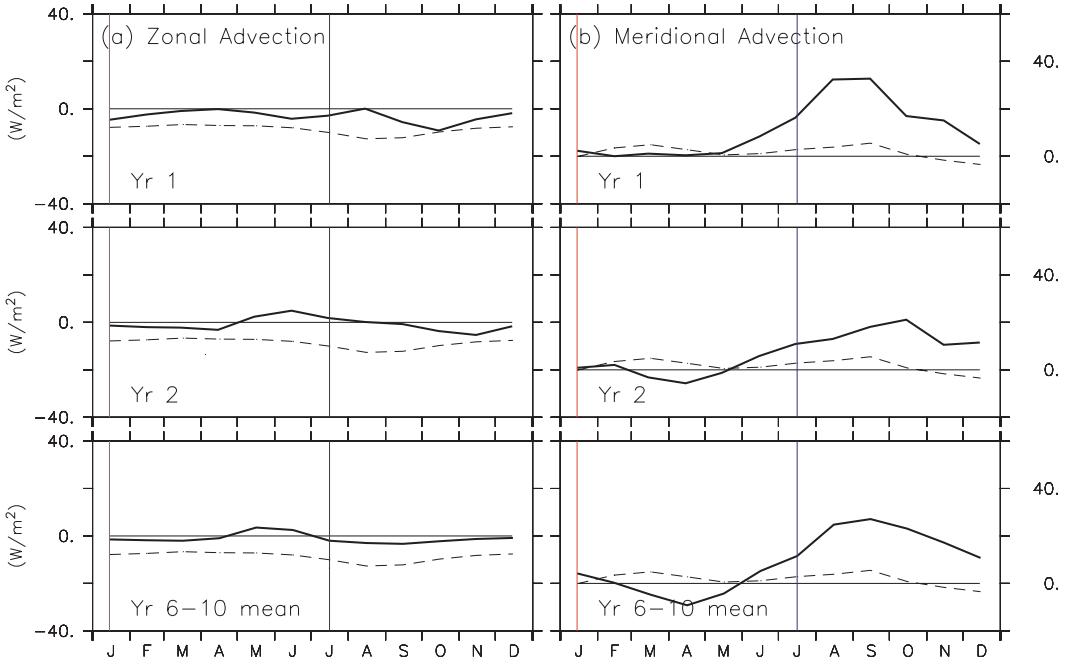

FIG. 6. As in Fig. 4 but for (a) zonal and (b) meridional heat transport.

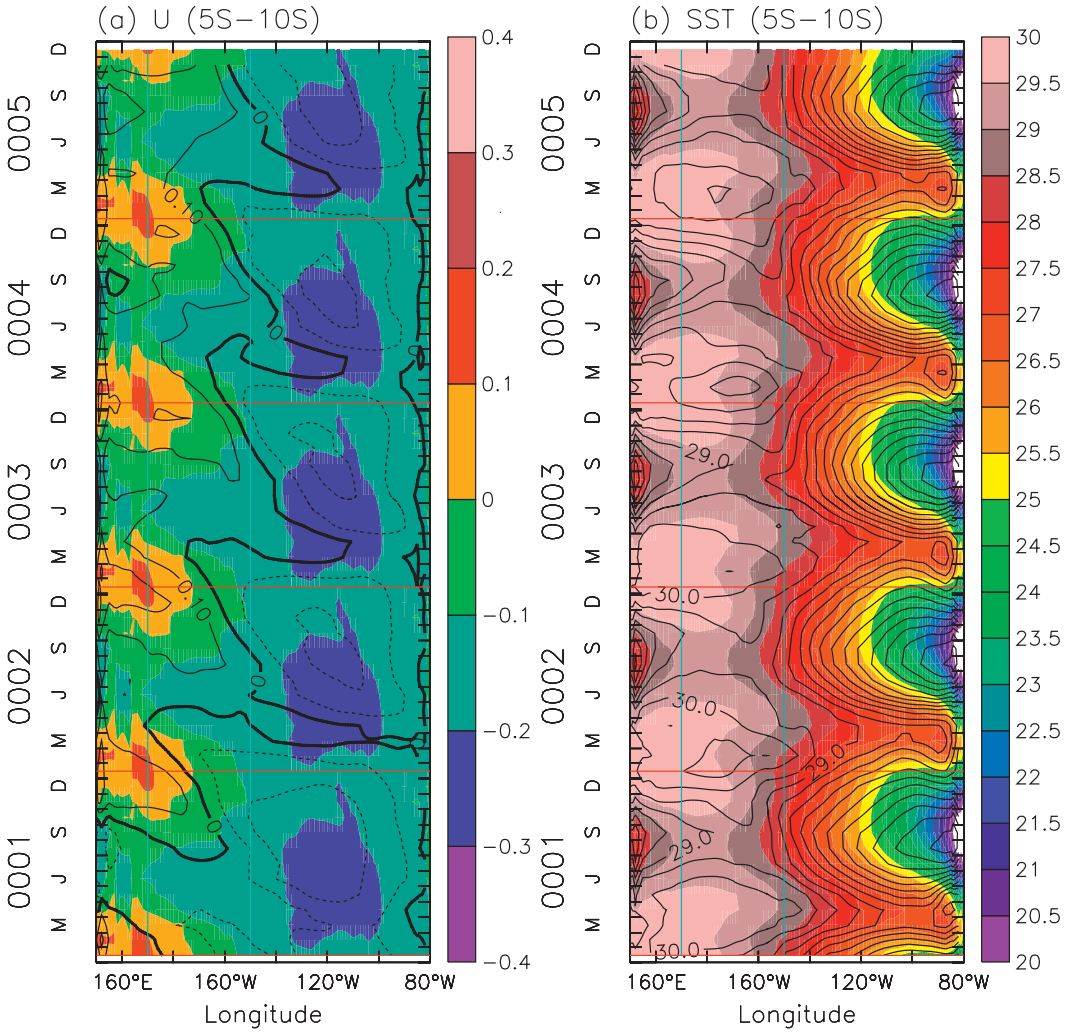

FIG. 7. Time–longitude diagram of (a) the surface zonal velocity (m s^{-1}) and (b) SST (°C), averaged between 10° and 5°S for the observation (shaded) and the first five years of CCSM ensemble mean (contours). January of each year is marked in red, and the region between the two cyan lines denotes the study domain.

c. *Initial bias*

In the previous section we found that the excessive shortwave radiation in the southern summer caused the initial warm bias. Since this occurred before the SST bias was developed, we expect this error to be associated with the atmospheric model.

Figure 10a shows the errors of solar radiation from the stand-alone atmospheric model of CCSM3 for January by using the data described in section 2. A center of positive bias with a magnitude about 40 W m^{-2} is found just over the region of warm SST bias in the south-central equatorial Pacific in January. A positive bias with the same pattern can also be found in the first month of the coupled integration (Fig. 10b). This indicates that the bias of the surface solar radiation can be primarily attributed to the atmospheric model.

The magnitudes of the biases of the solar radiation in CCSM are significantly smaller than that of the stand-alone atmospheric model in July (Figs. 10c and 10d). This is because in the coupled model, clouds respond to the warm SST biases, which is a negative feedback to the SST.

To corroborate the positive bias of the solar radiation, we also examined the properties of simulated clouds. Figure 11a shows the errors of total cloud amount from CAM against the observation from ISCCP D2 in January. A center of negative biases around 5% occurs over the study domain. This negative error allows more solar radiation arriving at the surface. The negative errors in the coupled model, however, are much reduced owing to the response of the cloud to the surface warm bias (Fig. 11b). The deficient cloud amount in the CAM is reflected

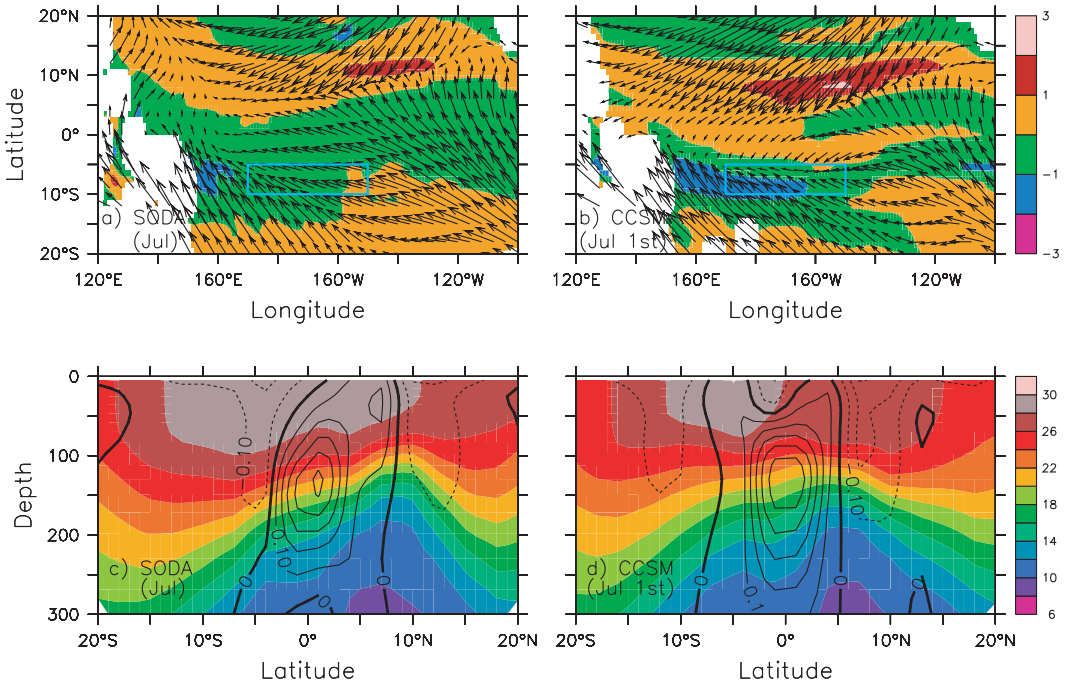

FIG. 8. The surface wind stress (vectors, dyn m^{-2} or 10^{-5} N m^{-2}) and the curl of wind stress (shaded, 10^{-6} dyn m^{-3}) for (a) the climatology of SODA in July and (b) CCSM ensemble mean in July of the first-year integration. The zonal mean sea temperature (shaded, °C) and zonal current (contours, m s^{-1}) between 170°E and 150°W from (c) SODA in July and (d) CCSM ensemble mean in July of the first-year integration. The cyan box from 5° to 10°S denotes the domain in which the heat budget is computed.

in the total gridbox cloud liquid water path (CLWP), which is more directly related to the excessive surface solar radiation. Figure 12a is the errors of the total gridbox CLWP from CAM versus the observation from SSM/I in January. In the study domain the negative bias is about 80 g m^{-2}. Less liquid water in cloud leads to more solar radiation reaching the surface. In CCSM, the pattern and magnitude of the negative biases are similar

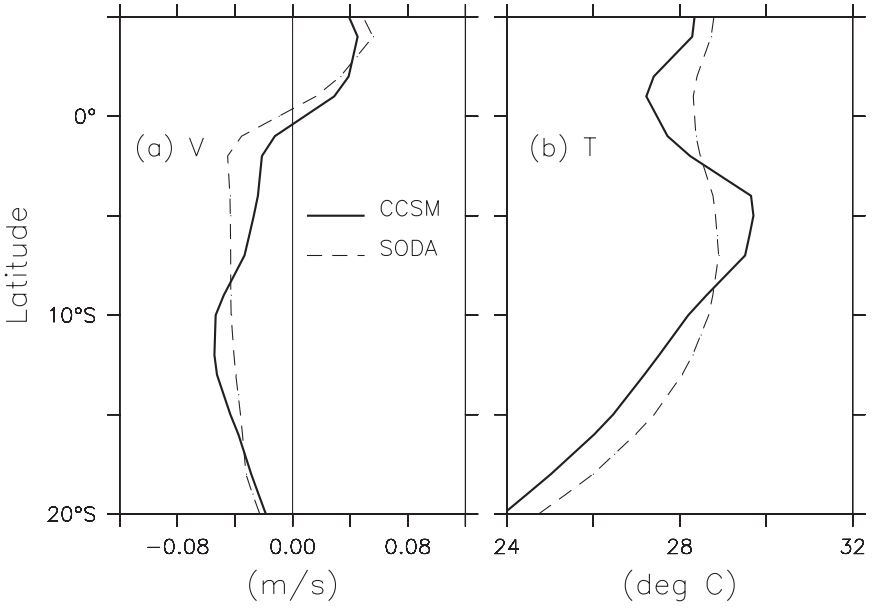

FIG. 9. The zonal averaged (a) surface meridional velocity (m s^{-1}) and (b) SST (°C) between 170°E and 150°W in July for SODA (dashed) and the first year of CCSM ensemble mean (thick).

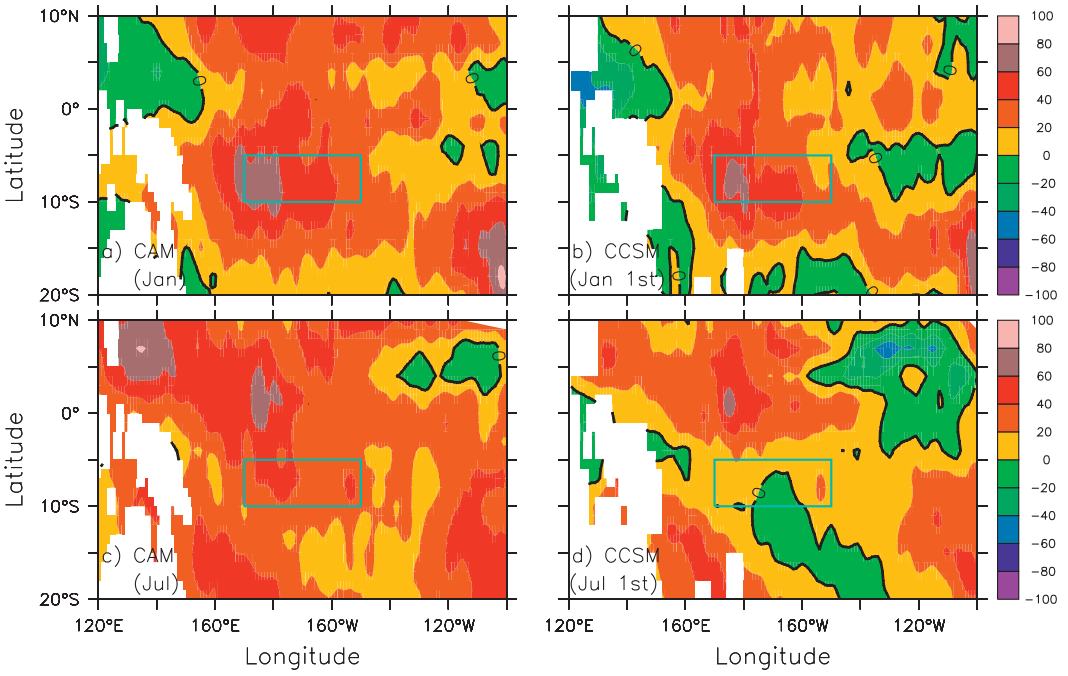

FIG. 10. The differences in surface solar radiation between the model and NOCS1a (W m^{-2}) for (a) January and (c) July from the climatology of AMIP run of CAM and for the (b) first and (d) seventh month of CCSM ensemble mean. The box from 5° to 10°S denotes the domain in which the heat budget is computed.

to those in stand-alone CAM (Fig. 12b). The analyses above clearly indicate that the underestimated cloud liquid water path contributed to the bias of initial surface radiative flux in CCSM.

d. The feedback loop

To understand the interactive role of the latent heat flux with SST, we use Fig. 13 to show the errors in the latent heat flux (shaded) and the magnitude of surface wind stress (contour) in the first and seventh month of the ensemble mean. In the figure, a positive value in latent heat flux means more heat to the ocean. The relationship between the two variables is quite distinct: larger wind stress corresponds to more cooling of the surface by latent heat flux. The relationship of the latent heat flux with the moisture difference with the surface air is much less clear. So, it is the errors in the surface wind that caused errors in the latent heat flux. In January the weak wind speed results in less latent heat released into the atmosphere over the south-central equatorial Pacific in both the CAM and the CCSM, contributing to the ocean warming as shown earlier. In July, however, the surface wind stress south of the study domain is significantly larger than in the CAM, which caused

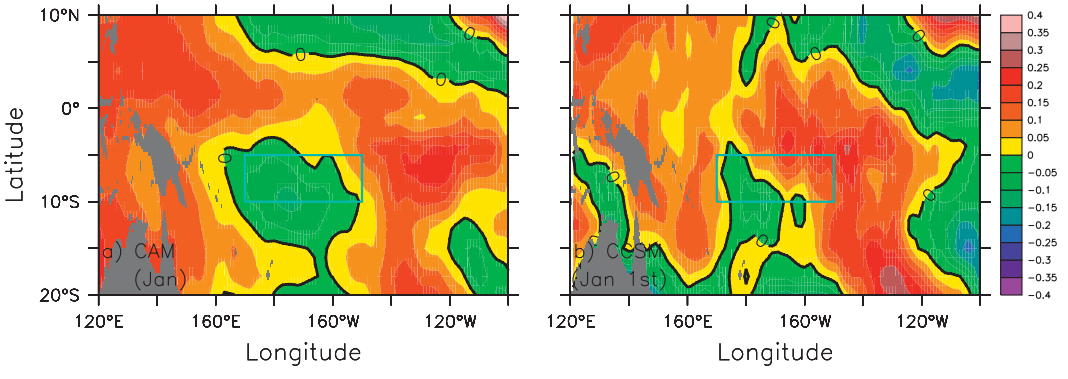

FIG. 11. Differences in total cloud amount between the model and ISCCP D2 (%) for (a) January from the climatology of AMIP run of CAM and (b) the first month of CCSM ensemble mean. The box from 5° to 10°S denotes the domain in which the heat budget is computed.

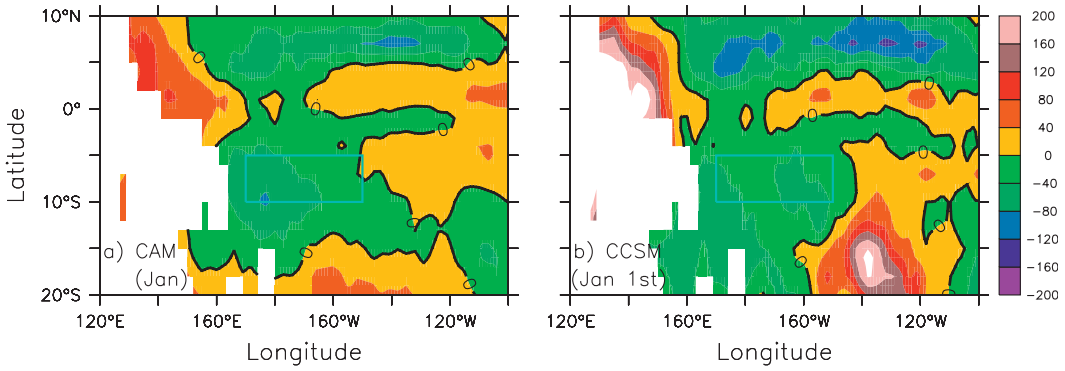

FIG. 12. As in Fig. 11 but for total gridbox cloud liquid water path (g m^{-2}). The observation is from SSM/I.

excessive evaporation that serves to cool the SST. The difference between the CAM and CCSM implies that this excessive surface wind stress is related to biases in SST.

This interactive response of the surface wind can be more clearly seen in Fig. 14, which shows the errors in the vector of surface wind stress in the first and seventh month of the AMIP run and the control run. Biases of the sea surface temperature for the CCSM are also presented in Fig. 14. The wind bias in the CCSM in the study region is similar to that in the AMIP run of CAM in January (Figs. 14a and 14b). But it has become much larger in July when large warm bias of SST developed at 5°S and a cold SST bias developed south of the study domain (Figs. 14c and 14d). Figures 13 and 14 also show that the cold bias in southern latitudes is likely caused by the excessive evaporation associated with the warm SST bias near the double ITCZ. Combining Figs. 13 and 14, we can see that the warm biases in SST, the convergence of surface wind, small wind speed, and the negative biases in latent heat flux are consistent with each other. The surface wind near the study region therefore has a positive feedback to the increasing temperature gradient between cold and warm biases. This feedback is also responsible for the change of the orientation of the warm band south of the equator.

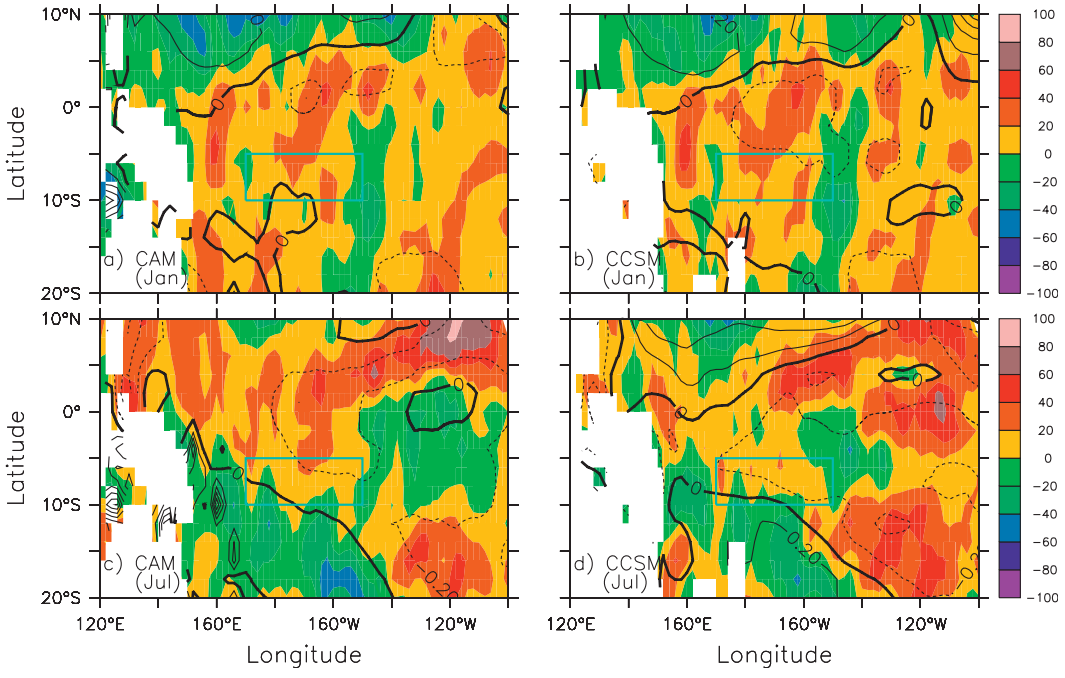

FIG. 13. Differences in latent heat flux (shaded, W m^{-2}) and the magnitude of surface wind stress (contours, dyn cm^{-2}) between model results and observations (NOCSa1 and SODA) for (a) January and (c) July from the climatology of AMIP run of CAM and for (b) first and (d) seventh month of CCSM ensemble mean. The box from 5° to 10°S denotes the domain in which the heat budget is computed.

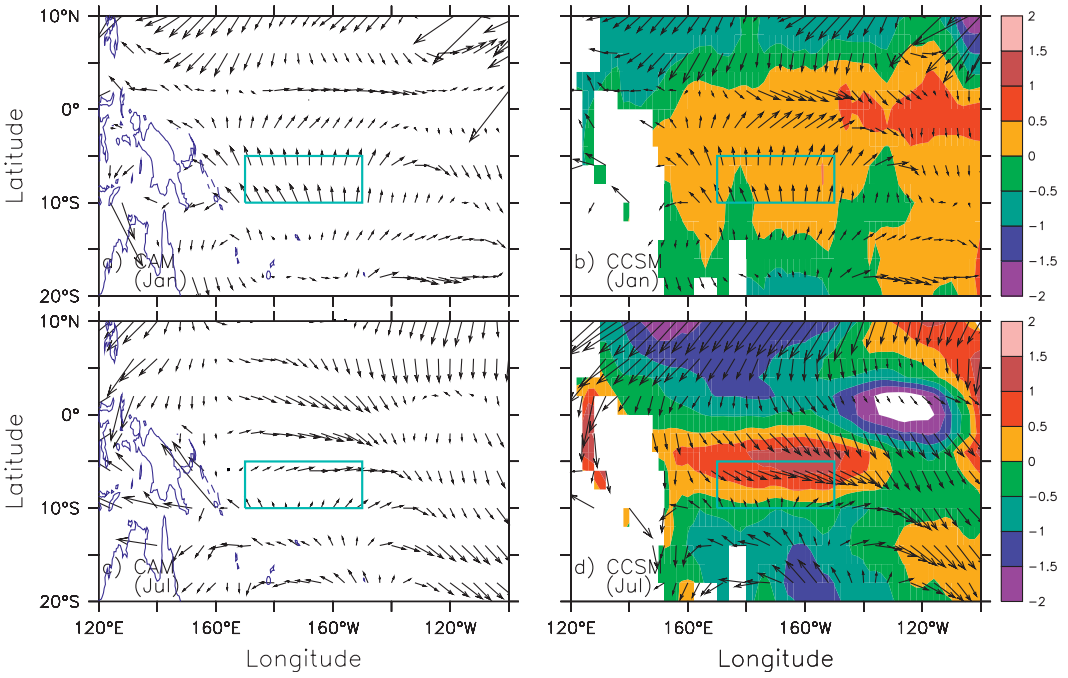

FIG. 14. Differences in the surface wind stress (vectors, dyn cm^{-2}) between model results and SODA for the (a) first and (c) sixth month of the AMIP run of CSM and for the (b) first and (d) seventh month of CCSM ensemble mean with the SST biases (shaded, °C). The box from 5° to 10°S denotes the domain in which the heat budget is computed.

To complete the feedback loop from ocean currents, we can use Figs. 8a and 8b to show the surface wind stress (vectors) and wind stress curl (shade) in July for SODA and for the first year of the control simulation, respectively. The corresponding latitude–depth section of zonal mean temperature (shade) and zonal currents (contour) in the central equatorial Pacific are shown in Figs. 8c and 8d. The zonal currents, thermocline shape, and the surface wind pattern in the model are all similar to Zhang et al. (2007). Due to the convergence of the surface wind over warm water, the positive wind curl occurs to the north of the study domain and the negative wind curl to the south. This makes the zero line of the wind stress curl lie just around the center of the study domain (Fig. 8b). Meanwhile, a spurious thermocline ridge, associated with the eastward current, has developed around 10°S (Fig. 8d).

e. *The c_0 experiment*

To investigate the role of excessive solar radiation in causing the warm bias, a sensitivity experiment is conducted with the solar radiation being reduced by arbitrarily increasing CLWP in the tropics (30°S–30°N) (the c_0 experiment). Figure 15a shows the difference of the total gridbox CLWP between c_0 and the control experiment in January. The CLWP increases in the western tropical Pacific Ocean. The surface solar radiation is reduced by approximately 60 W m^{-2} over the two positive CLWP centers south of the study domain. This reduction entirely offsets the excessive solar radiation in the beginning of the control simulation (Fig. 10b). The averaged surface solar radiative flux for the c_0 run over the study domain is 216 W m^{-2} in January, which is slightly less than the observation. In July, the large positive anomaly of CLWP in the western Pacific reduces the solar radiation by about 40 W m^{-2} (Fig. 15b).

Because of the reduction of shortwave radiation, the SST for the c_0 experiment in the tropics is reduced throughout the tropic Pacific basin (Fig. 16). The maximum cooling (about 1°C) in the open ocean occurs just over the study domain (Fig. 16b). This indicates that the double ITCZ, in terms of the warm SST bias in the south-central equatorial Pacific, is largely alleviated in the c_0 experiment when the surface solar radiation is reduced.

The improvement is also found in surface zonal currents. Due to the improvement of the surface wind, the spurious SECC in the c_0 experiment does not appear in the simulation (Fig. 17), while the SECC is developed in year 2 of the control run (Fig. 7a). This sensitivity experiment further confirms our interpretation of the initial development and maintenance of the double ITCZ in the model.

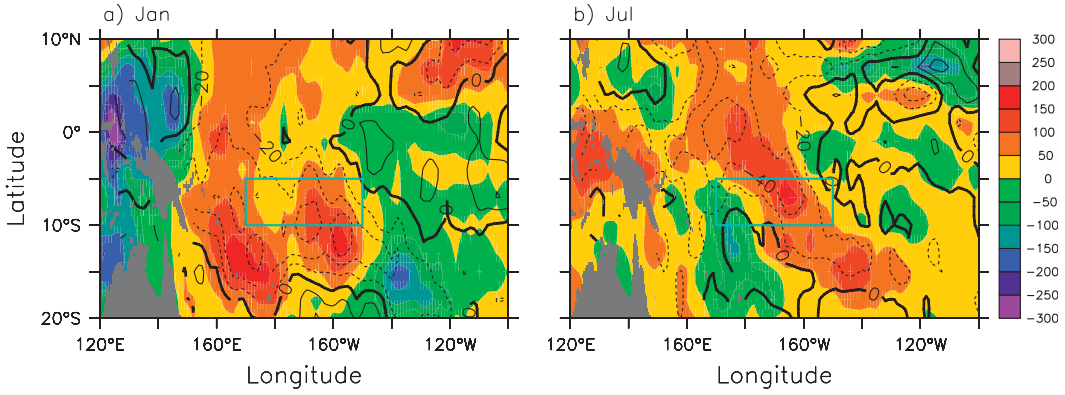

FIG. 15. Difference of the total gridbox cloud liquid water path (shaded, g m^{-2}) and the surface solar radiation (contour, W m^{-2}) between the c_0 and control run for (a) January and (b) July in first year of the integration.

4. Summary and discussion

We have presented an analysis of the initial development of the warm SST biases in the double ITCZ of the CCSM3 as a case study. The double ITCZ developed in the first year of the simulation, and the controlling processes equilibrated after the second year. Three key processes have been identified. First, an initial bias in the shortwave surface radiation, which can be traced to the stand-alone atmospheric model CAM, is responsible for the initial SST bias in austral summer. Second, in subsequent months the warm SST bias near the equator and the cold SST bias to the south, which is caused by the excessive latent heat flux, produce a spurious warm advection in the meridional direction that maintained the warm SST bias. Third, an eastward zonal current is set up as a result of the thermocline response to surface winds to advect warm water from west to east, which is opposite to the cold advection by the westward current in the observation. The excessive surface heat flux is partially offset by different surface components in different seasons of the year, but the bias in the ocean heat transport remains throughout the year. The spurious eastward current and its related zonal heat transport are consistent with the hypothesis proposed by Zhang et al. (2007).

In this study, we have initialized the model at the beginning of the calendar year. A natural question is whether the double ITCZ would develop similarly if the model were initialized in a different season. An additional experiment, started from July, has been conducted. The heat budget analysis indicates that the development of the warm SST bias also starts from January, the austral summer. The excessive shortwave radiation is also responsible for causing the initial warm SST bias in the south-central equatorial Pacific. Horizontal heat transport also contributes to maintaining the warm bias.

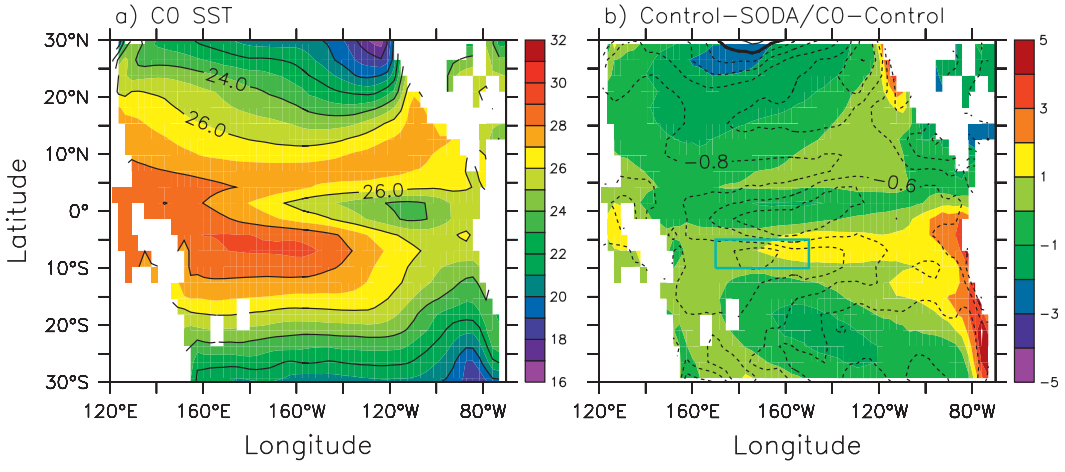

FIG. 16. (a) Annual-mean sea surface temperature (°C) for the c_0 experiment (years 6–10 mean) and (b) the difference of annual mean sea surface temperature between the c_0 and the control run of CCSM (years 6–10 mean, contours) and between the control run of CCSM and observation from SODA (1993–2004). The box in (b) from 5°S to 10°S, 170° to 150°E denotes the domain in which the heat budget is computed.

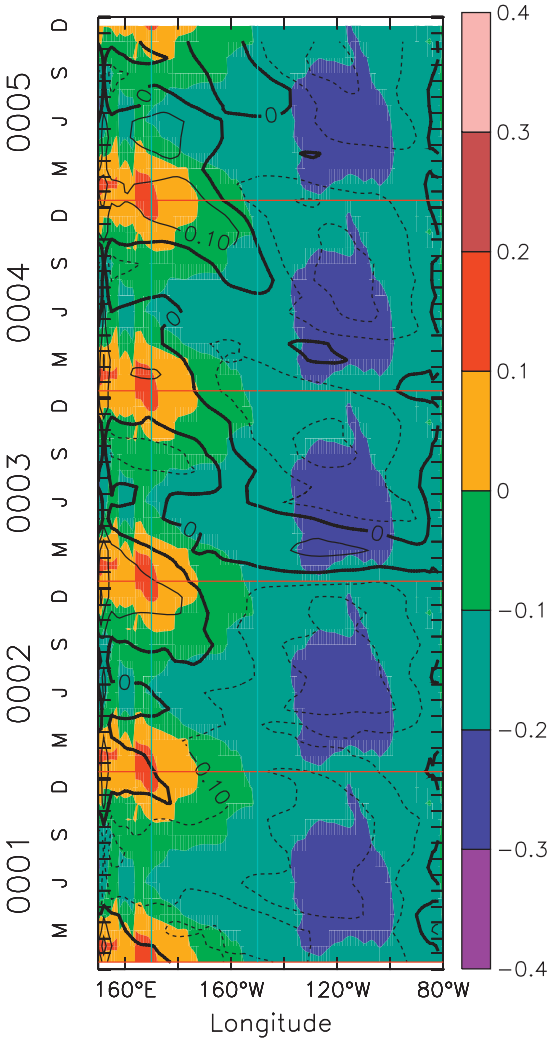

FIG. 17. As in Fig. 7a but for the c_0 experiment.

The double ITCZ is a common problem to coupled ocean–atmosphere models. Is the present analysis valid for models other than the CCSM? The overestimation of surface shortwave radiation is a long-standing problem in climate models. Whether this is due to insufficient absorption of solar radiation in clouds, or insufficient cloud amount or aerosols, is not clear. The solar radiation only causes an initial warm bias in the current analysis. In other models, there can be other causes of biases from surface winds or latent heat flux as a result of precipitation biases. The positive feedback mechanism of the oceanic advection with SST however is presumed to be generally applicable, and our analysis suggests that the feedback process can be set up within two years.

A legitimate question is why the positive feedback process does not lead to opposite SST biases since the initial bias can be negative, but almost all climate models simulate the double ITCZ. One explanation is that, when SST has a colder bias south of the equator, there is no similar response of surface winds to the SST biases because atmospheric convection does not occur when the SST is below certain threshold value. So, the zonal ocean current would not respond as strongly. Likewise, the response of the meridional wind will be smaller, and so is the meridional SST temperature gradient associated with surface evaporation. There is therefore likely an asymmetry in the consequences of positive and negative initial perturbations as a result of the asymmetry of the response of atmospheric convection to SST bias. A model therefore may have a preference to lock into a double ITCZ when there are episodes of both positive and negative perturbations.

This discussion however still cannot explain why double ITCZ is not in the observations. Two bands of warm SST and precipitation are actually often observed in the northern spring, but the southern branch dissipates going toward the northern summer. In the model, the meridional and zonal advection by the resolved ocean currents prevents the warm SST from dissipating. We presume that the horizontal heat transport process in the ocean in the equatorial region is different in the observation where small-scale and mesoscale eddies can be large episodically. Whether the seasonal variation of the horizontal subgrid-scale heat transport actually disrupts the persistence of the double ITCZ in the observation is a subject of future research.

Acknowledgments. We wish to thank the three anonymous reviewers for their valuable comments that have helped to improve our paper. This research is supported by the Climate Change and Prediction Program of the U.S. Department of Energy. Additional support is provided by NASA and the U.S. National Science Foundation to the Stony Brook University. This work was conducted during a visit of Hailong Liu to the Stony Brook University. Hailong Liu is also supported by the National Key Program for Developing Basic Sciences Grant 2010CB951904, and the National Natural Science Foundation of China under Grants 40775054, 41075059, and 41023002.

REFERENCES

Behringer, D., and Y. Xue, 2004: Evaluation of the global ocean data assimilation system at evaluation of the global ocean data assimilation system at NCEP: The Pacific Ocean. Preprints, *Eighth Symp. on Integrated Observing and Assimilation Systems for Atmosphere, Oceans, and Land Surface,* Seattle, WA, Amer. Meteor. Soc., 11–15.

Briegleb, B. P., C. M. Bitz, E. C. Hunke, W. H. Lipscomb, M. M. Holland, J. L. Schramm, and R. E. Moritz, 2004: Scientific

description of the sea ice component in the Community Climate System Model, version three. NCAR Tech. Rep. NCAR/TN463+STR, 78 pp.

Carton, J. A., and B. S. Giese, 2008: A reanalysis of ocean climate using simple ocean data assimilation (SODA). *Mon. Wea. Rev.,* **136,** 2999–3017.

Collins, W. D., and Coauthors, 2004: Description of the NCAR Community Atmosphere Model (CAM3). NCAR Tech. Rep. NCAR/TN-464+STR, 226 pp.

——, and Coauthors, 2006a: The Community Climate System Model version 3 (CCSM3). *J. Climate,* **19,** 2122–2143.

——, and Coauthors, 2006b: The formulation and atmospheric simulation of the Community Atmosphere Model version 3 (CAM3). *J. Climate,* **19,** 2144–2161.

Dai, F., R. Yu, X. Zhang, Y. Yu, and J. Li, 2003: The impact of low-level cloud over the eastern subtropical Pacific on the ''double ITCZ'' in LASG FGCM-0. *Adv. Atmos. Sci.,* **20,** 461–474.

Dickinson, R. E., K. W. Oleson, G. Bonan, F. Hoffman, P. Thornton, M. Vertenstein, Z.-L. Yang, and X. Zeng, 2006: The Community Land Model and its climate statistics as a component of the Community Climate System Model. *J. Climate,* **19,** 2302–2324.

Gent, P., and Coauthors, 2011: The Community Climate System Model Version 4. *J. Climate,* **24,** 4973–4991.

Grist, J., and S. Josey, 2003: Inverse analysis adjustment of the SOC air–sea flux climatology using ocean heat transport constraints. *J. Climate,* **16,** 3274–3295.

Large, W. G., and G. Danabasoglu, 2006: Attribution and impacts of upper-ocean biases in CCSM3. *J. Climate,* **19,** 2325–2346.

Lee, T., I. Fukumori, and B. Tang, 2004: Temperature advection: Internal versus external processes. *J. Phys. Oceanogr.,* **34,** 1936–1944.

Levitus, S., and T. P. Boyer, 1994: *Temperature*. Vol. 4, *World Ocean Atlas 1994,* NOAA Atlas NESDIS 4, 117 pp.

——, R. Burgett, and T. P. Boyer, 1994: *Salinity*. Vol. 3, *World Ocean Atlas 1994,* NOAA Atlas NESDIS 3, 99 pp.

Lin, J., 2007: The double-ITCZ problem in IPCC AR4 coupled GCMs: Ocean–atmosphere feedback analysis. *J. Climate,* **20,** 4497–4525.

Lin, P. F., H. L. Liu, and X. H. Zhang, 2007: Sensitivity of the upper ocean temperature and circulation in the equatorial Pacific to solar radiation penetration due to phytoplankton. *Adv. Atmos. Sci.,* **24,** 765–780.

Liu, H., W. Lin, and M. Zhang, 2010: Heat budget of the upper ocean in the south-central equatorial Pacific. *J. Climate,* **23,** 1779–1792.

Ma, C., C. Mechoso, A. Robertson, and A. Arakawa, 1996: Peruvian stratus clouds and the tropical Pacific circulation: A coupled ocean-atmosphere GCM study. *J. Climate,* **9,** 1635–1645.

Mechoso, C. R., and Coauthors, 1995: The seasonal cycle over the tropical Pacific in coupled ocean–atmosphere general circulation models. *Mon. Wea. Rev.,* **123,** 3825–3838.

Oleson, K. W., and Coauthors, 2004: Technical description of the Community Land Model (CLM). NCAR Tech. Rep. NCAR/TN-461+STR, 174 pp.

Paulson, C., and J. Simpson, 1977: Irradiance measurements in the upper ocean. *J. Phys. Oceanogr.,* **7,** 952–956.

Rosati, A., and K. Miyakoda, 1988: A general circulation model for upper-ocean circulation. *J. Phys. Oceanogr.,* **18,** 1601–1626.

Rossow, W. B., A. W. Walker, D. E. Beuschel, and M. D. Roiter, 1996: International Satellite Cloud Climatology Project (ISCCP) documentation of new cloud datasets. World Meteorological Organization Rep. WMO/TD 737, 115 pp.

Smith, R. D., and P. R. Gent, 2002: Reference manual for the Parallel Ocean Program (POP), ocean component of the Community Climate System Model (CCSM2.0 and 3.0). Los Alamos National Laboratory Tech. Rep. LA-UR-02-2484, 73 pp.

Song, X., and G. J. Zhang, 2009: Convection parameterization, tropical Pacific double ITCZ, and upper-ocean biases in the NCAR CCSM3, Part I: Climatology and atmospheric feedback. *J. Climate,* **22,** 4299–4315.

Wentz, F. J., 1997: A well-calibrated ocean algorithm for SSM/I. *J. Geophys. Res.,* **102,** 8703–8718.

Wunsch, C., and P. Heimbach, 2007: Practical global ocean state estimation. *Physica D,* **230,** 197–208, doi:10.1016/j.physd.2006.09.040.

Xie, S.-P., and S. G. H. Philander, 1994: A coupled ocean–atmosphere model of relevance to the ITCZ in the eastern Pacific. *Tellus,* **46A,** 340–350.

Yu, J. Y., and C. R. Mechoso, 1999: Links between annual variations of Peruvian stratocumulus clouds and of SST in the eastern equatorial Pacific. *J. Climate,* **12,** 3305–3318.

Zhang, G. J., and N. A. McFarlane, 1995: Sensitivity of climate simulations to the parameterization of cumulus convection in the Canadian Climate Centre general circulation model. *Atmos.–Ocean,* **33,** 407–446.

——, and H. J. Wang, 2006: Toward mitigating the double ITCZ problem in NCAR CCSM3. *Geophys. Res. Lett.,* **33,** L06709, doi:10.1029/2005GL025229.

——, and X. Song, 2010: Convection parameterization, tropical Pacific double ITCZ, and upper-ocean biases in the NCAR CCSM3. Part II: Coupled feedback and the role of ocean heat transport. *J. Climate,* **23,** 800–812.

Zhang, M. H., 1996: Implication of the convection-evaporation-wind feedback to surface climate simulation in climate models. *Climate Dyn.,* **12,** 299–312.

Zhang, X., W. Lin, and M. Zhang, 2007: Toward understanding the double intertropical convergence zone pathology in coupled ocean-atmosphere general circulation models. *J. Geophys. Res.,* **112,** doi:10.1029/2006JD007878.